Real-time GNSS NLOS Detection and Correction Aided by Sky-Pointing Camera and 3D LiDAR

Xiwei Bai[1], Weisong Wen[2*], Guohao Zhang[1], Li-Ta Hsu[1]
[1]*Interdisciplinary Division of Aeronautical and Aviation Engineering, The Hong Kong Polytechnic University*
[2]*Department of Mechanical Engineering, The Hong Kong Polytechnic University*

BIOGRAPHY (IES)

Xiwei Bai is currently a research assistant in Hong Kong Polytechnic University. Her research topic is GNSS positioning aided by computer vision, object detection and recognition using machine learning.

Guohao Zhang received the bachelor's degree in mechanical engineering and Automation from University of Science and Technology Beijing, China, in 2015. He received the master's degree in mechanical engineering and currently is a Ph.D. student in the Hong Kong Polytechnic University. His research interests include GNSS urban localization, vehicle-to-vehicle cooperative localization and multi-sensor integrated navigation.

Weisong WEN is currently a PhD candidate in mechanical engineering, the Hong Kong Polytechnic University. His research interests include the multi-sensor integrated localization for autonomous vehicles, 3DLiDAR aided GNSS positioning and SLAM. In 2018, he was a visiting researcher in Mechanical Systems Control (MSC) Lab of University of California, Berkeley (UCB).

Li-Ta Hsu is an Assistant Professor in the Division of Aeronautical and Aviation Engineering at Hong Kong Polytechnic University. Dr Hsu has been member of Editorial Board in GPS Solutions since 2015. He is an Associate Fellow of RIN. From 2014 to 2016, he was a postdoctoral researcher at the University of Tokyo, after his stay in Tokyo Marine University as visiting researcher. From 2012 to 2013, he was a visiting researcher in University College London. He received BSc and PhD degree in Aeronautics and Astronautics from National Cheng Kung University, Taiwan, in 2007 and 2013, respectively. His technical expertise and interests include the detection, mitigation and correction of GNSS multipath and NLOS effects to improve GNSS positioning performance in the super-urbanized cities using 3D Mapping Aided GNSS, 3D LiDAR Aided GNSS and Vector Tracking approaches.

ABSTRACT

Robust and globally referenced positioning is the basis of fully autonomous driving in diverse scenarios. Globally navigation satellite system (GNSS) is currently the main source providing globally referenced positioning. Satisfactory accuracy (5~10 meters) can be obtained in sparse areas. However, the GNSS positioning error can go up to even 100 meters in dense urban areas due to the multipath effects and none-line-of-sight (NLOS) reception caused by reflection and blockage from buildings. NLOS is currently the dominant component degrading the performance of GNSS positioning. Recently, the camera is employed to detect the NLOS satellites and then the NLOS are excluded from GNSS calculation. This exclusion can cause severe distortion of satellite distribution, due to the excessive NLOS receptions in deep urban canyon. This paper proposes to correct the NLOS receptions with the aid of 3D LiDAR ranging after detecting NLOS receptions using camera. The sky-pointing monocular camera is firstly employed to detect satellite visibility. Then, the NLOS delay is modeled using the satellite elevation angle, azimuth angle and distance from receiver to possible reflector which is ranged by 3D LiDAR. The pseudorange measurements are corrected using the estimated NLOS delay. Finally, the GNSS positioning is improved using corrected pseudorange measurements and healthy (visible) satellites. The proposed method is verified through real road tests in a deep urbanized canyon of Hong Kong. The result shows that the proposed method can effectively improve the GNSS positioning performance by decreasing the mean error from 22.01 to 14.96 meters.

1. INTRODUCTION

Autonomous vehicle [1] is believed to be a remedy to reduce the excessive traffic jams and accidents. Insufficient positioning accuracy is one of the key problems that postponing the arrival of autonomous driving. Light detection and ranging (LiDAR), camera and inertial navigation system (INS) are usually integrated with GNSS positioning [2-4] to obtain more accurate and

robust positioning. However, the three positioning sources can only conduct relative positioning. GNSS receiver is the only one that can continually provide absolute positioning and possess increased popularity because of the availability of multi-constellation satellite navigation systems (GPS, BeiDou, GLONASS, Galileo and QZSS). GNSS positioning can provide satisfactory performance if GNSS receiver receives enough direct signals transmitted from satellites. However, the GNSS transmission may be reflected, diffracted or blocked by surrounding buildings and moving objects [5] in dense urban canyon, such as Hong Kong, which can cause additional signal transmission delay. Thus, it introduces pseudorange errors due to both multipath effect and none-light-of-sight (NLOS) reception. If the direct light-of-sight (LOS) is blocked and reflected signals from the same satellite are received, the notorious non-light-of-sight (NLOS) receptions occurred. This NLOS dominants the GNSS positioning errors in the dense urban. As a result, the positioning error can go up to even 100 meters [6, 7].

According to a recent review paper [8], NLOS is currently the major difficulty to use GNSS in the applications of the intelligent transportation system in urbanized cities. As the majority of the NLOS receptions are caused by static buildings, various researches [9-11] utilize the 3D building models to identify the NLOS/LOS signals. Then, the NLOS receptions are excluded from further GNSS positioning. Interestingly, a recent research [5] shows that the dynamic vehicles can also cause GNSS NLOS and improvement is obtained by detecting and excluding NLOS receptions. However, excessive exclusion of NLOS measurements can significantly distort the satellite distribution as majority of the satellites are NLOS in dense urban. As a result, the GNSS positioning can be even worse after NLOS exclusion. An example of NLOS exclusion is given in Figure 1. The red curve indicates the satellite (GPS/BeiDou) number in a dense urban. After the NLOS exclusion, the satellite number (blue curve) decreases dramatically. More importantly, the value of parameter, horizontal dilution of precision (HDOP), which reflecting the quality of satellite distribution increases significantly. Therefore, NLOS exclusion in dense urban is not preferable.

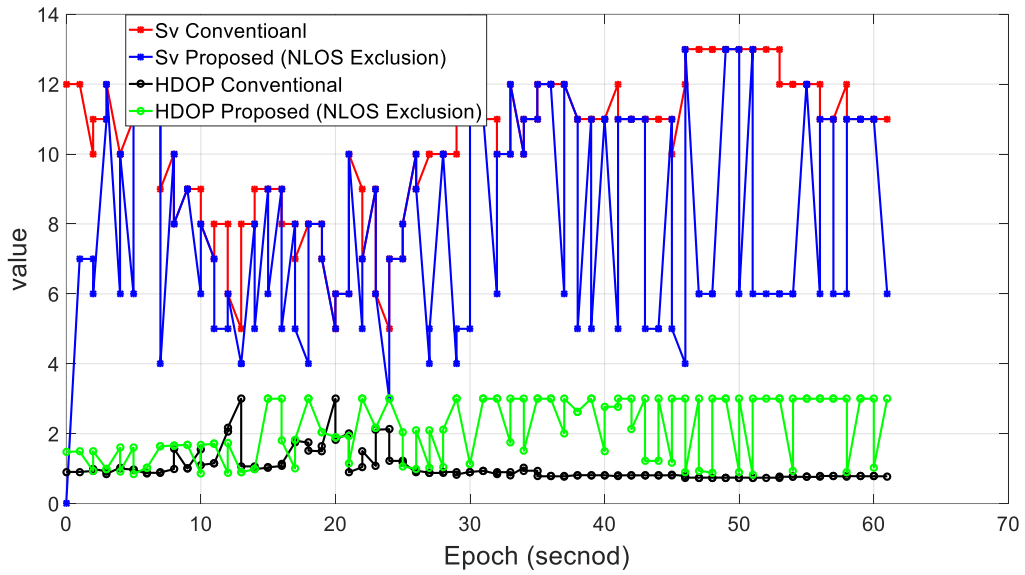

Fig. 1. Demonstration of numbers of satellite measurement before (red) and after (blue) NLOS exclusion in an urban canyon in Hong Kong. GPS and BeiDou signals are received by GNSS receiver.

A well-known method GNSS shadow matching is studied to match the measured satellite visibility with the predicted satellite visibility of hypothesized positions [12-14]. However, the performance of shadow matching relies on the quality of satellite visibility classification and initial guess of GNSS receiver. A likelihood-based 3DMA GNSS method, which modeled the measurement uncertainty to mitigate the NLOS and multipath effects, is also proposed to provide accurate positioning in the along-street direction [15]. Due to the complementariness of the shadow matching and the likelihood-based 3DMA GNSS, their integration is recently studied [16] to obtain better performance. Another stream of range-based 3DMA GNSS method is to correct the NLOS affected measurement for GNSS positioning [17-20]. These methods are proposed to simulate the signals transmission routes using the ray-tracing method [21]. However, the drawbacks of these ray-tracing based 3DMA GNSS methods are the stringent requirements on 1) the accuracy of 3D mapping database 2) the initial guess of receiver positions and 3) the computational power of the processors due to the ray-tracing process. Interestingly, the constructed map of the environment using 3D LiDAR is employed to classify the visibility of satellites. A research then modeled the GNSS noise covariance by NLOS detection based on LiDAR-constructed map [22]. A research incorporates LiDAR map and 3D city model to exclude NLOS is conducted in the application of unmanned aerial vehicle [23].

Recently, due to the fast development of computer vision technique, the camera is applied to capture the sky view to further identify the satellite visibility. To detect the visibility of satellites, the researchers apply omnidirectional and fisheye cameras

[24-26] to detect the sky views of the environment in the urbanized area. NLOS receptions can be detected with the detected sky views and some improvements are obtained. Similar researches [27, 28] are conducted recently and the improved GNSS positioning is integrated with visual simultaneous localization and mapping [29]. However, these methods still tend to exclude the NLOS receptions from further GNSS positioning which is not applicable in the dense urban areas, such Hong Kong, Tokyo and New York cities. In our team's previous work [30], we employ the 3D LiDAR and building height to correct the NLOS receptions. Improved GNSS positioning is obtained with the NLOS correction method. However, the performance of the method relies on the availability of buildings height.

This paper proposes to improve the GNSS single point positioning (SPP) by detecting the GNSS NLOS receptions, and then correcting the NLOS receptions with the aid of real-time point clouds from 3D LiDAR. The monocular camera is firstly applied to capture the sky view. The sky and non-sky areas are segmented using image processing method, and then the satellites are projected into the segmented image with the aid of heading angle of the camera provided by the E-compass. The satellite visibility can be identified using the Skyplot [31]. Instead of excluding the NLOS satellites, the NLOS pseudorange measurements are corrected using a NLOS transmission and reflection model proposed in the previous work by our team in [6]. Finally, the GNSS positioning is conducted using the healthy measurements and corrected measurements. The remainder of this paper is structured as follows. An overview of the proposed method is presented in Section 2. The NLOS detection method is presented in Section 3. The experiment evaluation is presented in Section 5 after the NLOS model being introduced in Section 4. Finally, the conclusions and future work are drawn in Section 6.

2. OVERVIEW OF THE PROPOSED METHOD

In this study, we propose to detect and correct the NLOS receptions caused by surrounding objects, such as buildings, trees, etc. Figure 2 presents direct propagation routes and possible NLOS receptions of GNSS signal. In the dense urban shown in Figure 2, the surrounding buildings can easily block the satellites with low elevation angles. However, the NLOS signals can also be reflected by the building surface on the other side. As a result, the NLOS reception is caused and can be received by GNSS receiver. To detect and correct the NLOS satellites, the proposed method can be executed as shown in Figure 3.

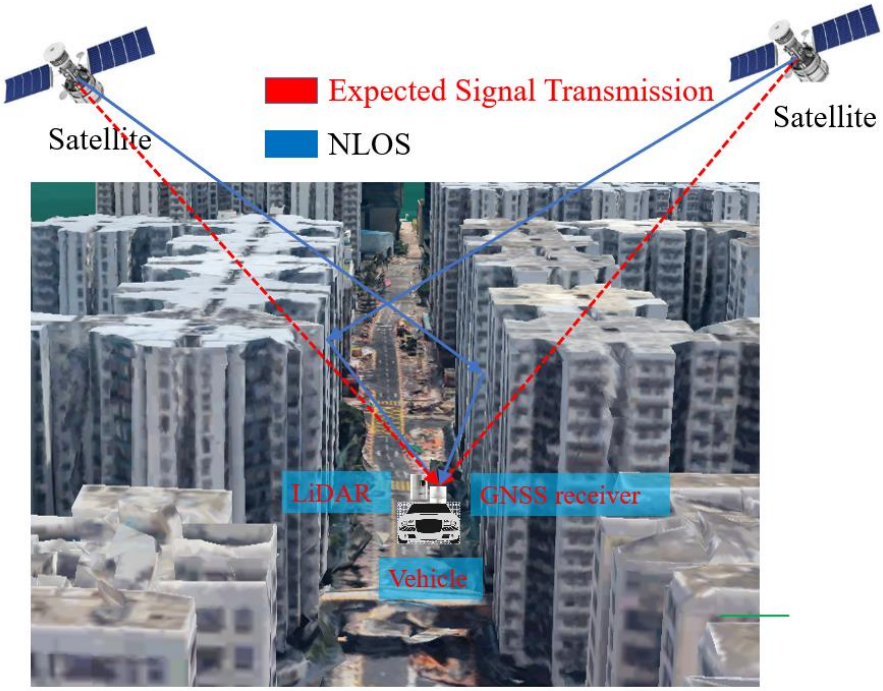

Fig.2 Illustration of NLOS receptions caused by surrounding buildings.

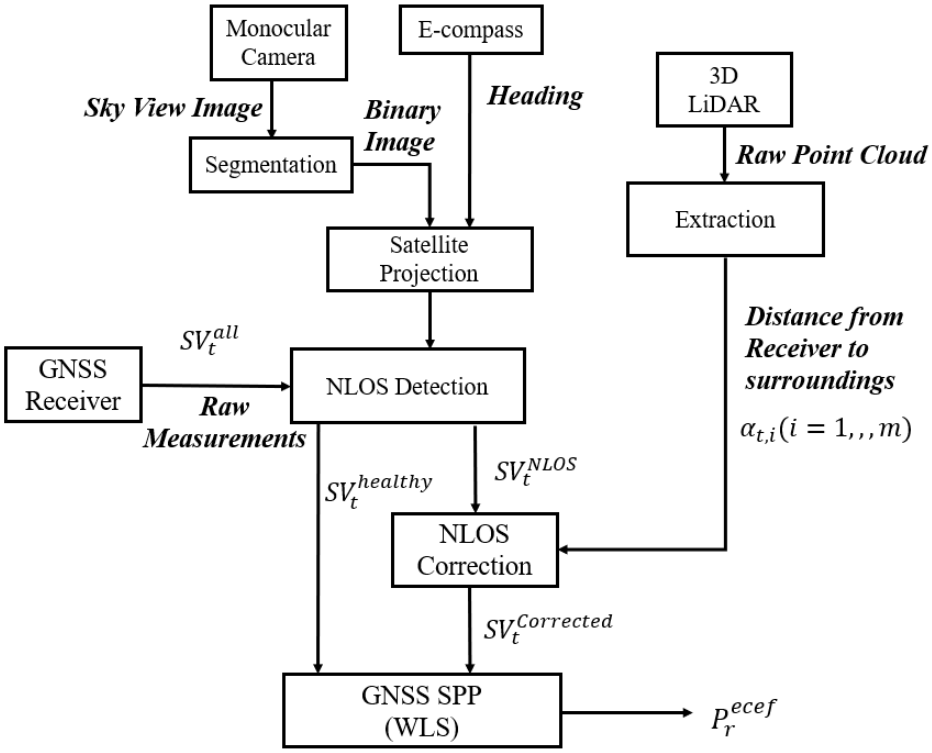

Fig.3 Overview of the proposed algorithm. The main inputs are GNSS raw measurements, sky view image from monocular camera and real-time point clouds from 3D LiDAR. The auxiliary inputs are yaw angle from E-compass.

As shown in Figure 3, the GNSS raw measurements including satellite elevation and azimuth angles, pseudorange measurements are obtained from GNSS receiver. The sky view image is collected using a sky-pointing monocular camera. The sky view image is segmented and projected into the GNSS elevation and azimuth angle coordinate with the aid of heading angle from E-compass. Then, the Skyplot is obtained. The LOS/NLOS can be classified using the perceived and segmented sky view. The 3D LiDAR provides the real-time point clouds of the surrounding and the distance ($\alpha_{t,i}$ with *t* indicating the epoch and *i* denoting the point ID) from the GNSS receiver to surroundings is extracted from the raw point clouds. The NLOS correction is then estimated using the elevation angle, azimuth angle of NLOS measurements, and $\alpha_{t,i}$ using the NLOS model in [6]. Finally, the GNSS SPP is conducted using weighted least square (WLS) using both healthy and corrected pseudorange measurements.

3. NLOS DETECTION USING MONOCULAR CAMERA

The sky view image can effectively represent the geometry distribution of surrounding objects. In this section, the image processing method is employed to segment the sky view image to further distinguish the sky area and non-sky area. Then, the satellite visibility is identified by projecting the satellites into the sky view image with the aid of camera's reference heading.

3.1 Sky View Segmentation

The sky view is captured using the monocular camera and is shown in Figure 4 (a). When a satellite has a higher elevation angle than top edge, it is regarded as visible. Otherwise, the satellite is invisible to GNSS receiver. Therefore, the main task for identifying satellite visibility lies to extract the top edge of the surrounding objects. In other words, the main problem is how to segment the sky area and non-sky area in the image. In this paper, we propose to use three steps to distinguish the sky area and non-sky area: (a). transform the color image to grayscale image. (b). transform the grayscale image to binary image with adaptive threshold. (c). removing the noisy points inside the binary image using median filtering algorithm. These functions are conducted using OpenCV [32] library. The grayscale image and binary image are shown in Figure 4 (b) and (c), respectively. We can see from the Figure 4 (c) that the proposed sky view segmentation method can effectively separate the sky and non-sky area (the sky area is white). If the satellite locates inside the sky area, the satellite is visible to the GNSS receiver and vice versa.

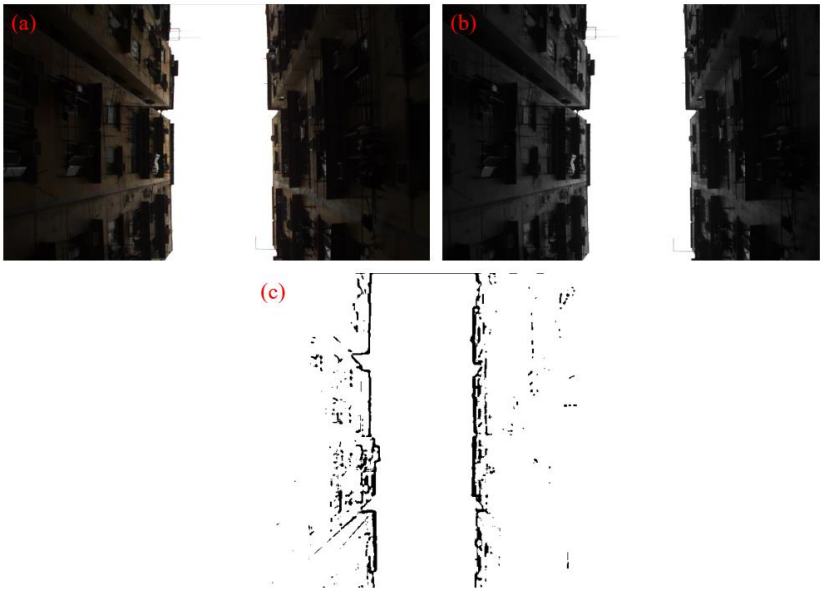

Fig.4 Illustration of sky view image segmentation. (a) raw image. (b) grayscale image. (c) binary image.

3.2 Satellite Projection and LOS/NLOS Classification

To identify the satellite visibility based on the segmented sky view image, the satellite needs to be projected to the image coordinate system. The illustration of projecting satellite into image is shown in Figure 5. For each satellite associated with specific azimuth and elevation angle, it possesses a pixel position inside the sky view image. We assume that the optical center of the camera is zenith pointing. To determine the position of the satellite inside the image, we need:

(a) The distance from the center of the sky view image in pixels ($\boldsymbol{r_{pix}}$) which is correlated to the elevation angle ($\boldsymbol{\emptyset_{sat}}$) of the satellite.

(b) The azimuth angle of the sky view image. The azimuth angle of satellite is globally referenced, thus the reference heading ($\boldsymbol{\tau_h}$) of the camera is needed to align the image plane coordinate and the north of the earth. Note that the reference heading is provided by the E-compass in this paper.

Assume that the satellite is projected into the image plane shown in Figure 5. The image plane coordinate system is identical to the image coordinate system. The r_{pix} shown in Figure 5 indicates the distance between the satellite position in the image and center of the image. The r_{pix} is determined by the satellite elevation angle and the focal length (f_c) of the monocular camera. The angle θ satisfies:

$$\theta = \frac{\pi}{2} - \emptyset_{\text{sat}} \tag{1}$$

Thus, we have r_{pix} being formulated as:

$$r_{\text{pix}} = f_c \tan(\frac{\pi}{2} - \emptyset_{\text{sat}}) \tag{2}$$

Given the center of the sky view image in pixel as (x_c, y_c), the position (x_s, y_s) of the given satellite inside the sky view image can be formulated as:

$$x_s = x_c + r_{pix} \cos(\tau_h + \alpha_{sat}) \tag{3}$$

$$y_s = y_c - r_{pix} \sin(\tau_h + \alpha_{sat}) \tag{4}$$

where the $\boldsymbol{\alpha_{sat}}$ is the azimuth angle of the satellite.

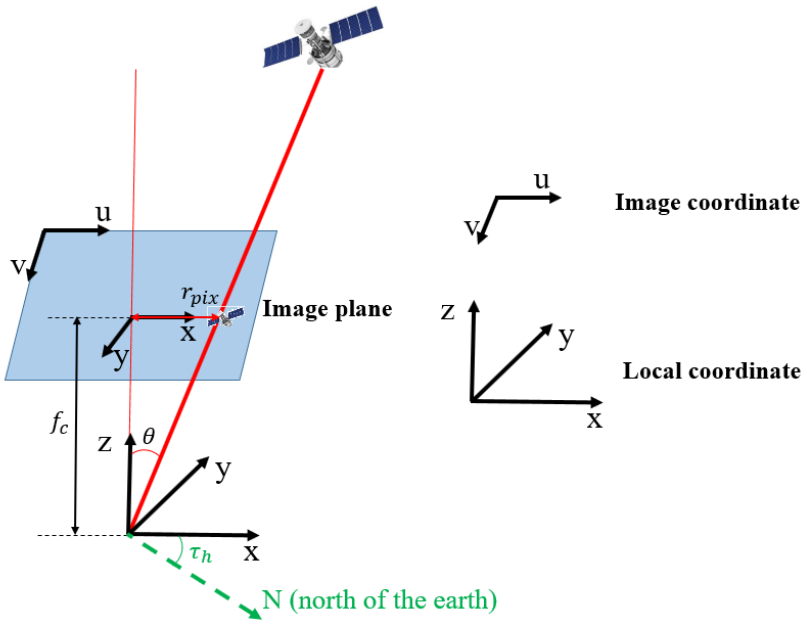

Fig.5 Illustration of projecting satellite into image.

After the satellite is projected into the sky view image as shown in Figure 4 (c), we propose a searching method to identify the satellite visibility. For a given satellite 1 (see Figure 6) positioning in pixel inside a sky view image, we propose to identify the visibility using Algorithm 1. $V_{threshod}$ indicates the threshold of mean pixel value and is experimentally determined.

Algorithm 1: Satellite Visibility Identification

Input: binary image I_t as shown in Figure 4(c), satellite position (x_s, y_s) in pixels inside the image
Output: satellite visibility st_v (visible: $st_v = 1$, invisible: $st_v = 0$)
Step 1: initialize the searching point (x_d, y_d) start from the center $((x_c, y_c))$ of the image I_t , $st_v = 1$, the searching direction denoted by angle ε (see Figure 6).
Step 2: given a constant incremental value Δd, the searching point is updated as follows:

$$x_d = x_d + \Delta d \cos(\varepsilon) \quad (5)$$
$$y_d = y_d - \Delta d \sin(\varepsilon) \quad (6)$$

Step 3: given the dynamic point (x_d, y_d) as the center of the searching circle, calculate the mean of pixel values of all the points inside the searching circle as follows:

$$\bar{V} = \sum_{i=1}^{m} I_t(x_{d,i}, y_{d,i}) \quad (7)$$

$I_t(x_{d,i}, y_{d,i})$ represents the pixel value of the point i inside the searching circle.

Step 4: if $\bar{V} > V_{threshod}$, set st_v to 0.
Step 5: Repeat Steps 2 and 3 until the dynamic point reaches the position (x_s, y_s) of the given satellite.

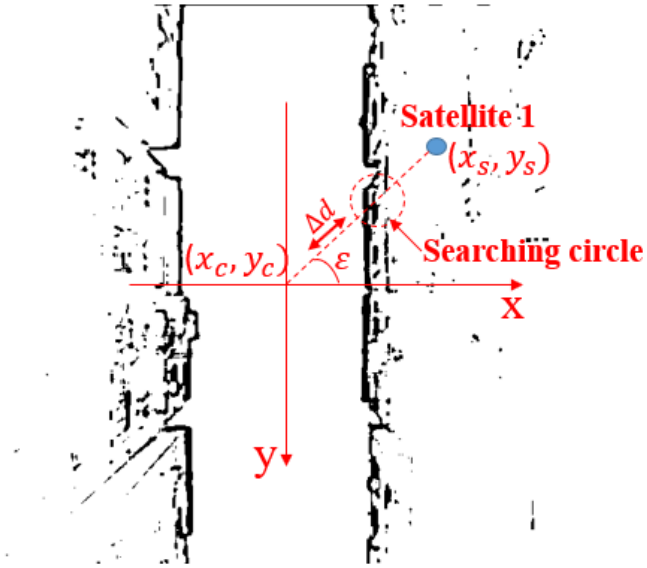

Fig.6 Illustration of satellite visibility identification based on the proposed method.

The classified satellite visibilities are shown in Figure 7 (a case in dense urban). Due to the limited field of view (FOV) of the applied monocular camera, the camera can only capture part of the surroundings (the part with high elevation angle can be captured). However, mean mask elevation angle can go up to ~50 degrees in dense urban, which means monocular camera (FOV: 45~90 degree) is actually enough for dense urban case. In total, 5 NLOS satellites (satellite 25, 93, 89, 10, 92) are identified and only one LOS satellite (satellite 27) in Figure 7.

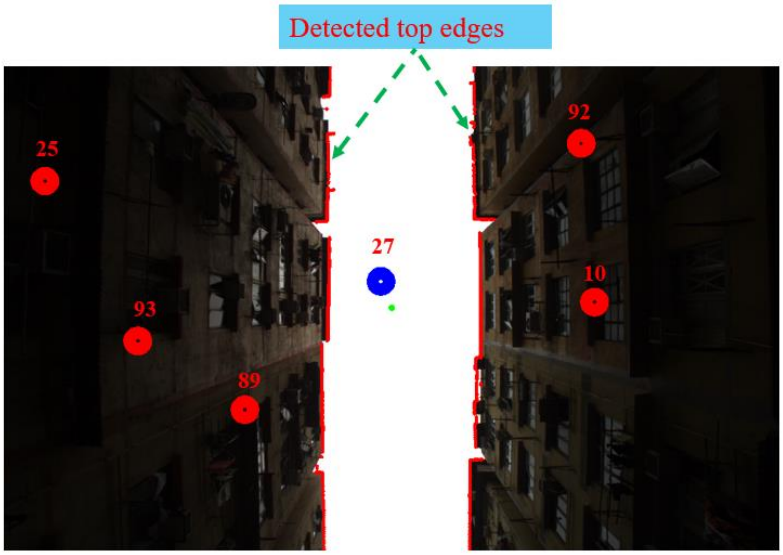

Fig.7 Illustration of identified satellite visibilities using proposed method. The blue and red circles denote the LOS and NLOS satellites, respectively. The red curve denotes the detected edge separating the sky and non-sky area. The number represents the satellite index (PRN).

4. IMPROVED GNSS POSITIONING WITH NLOS CORRECTION

In this section, NLOS error model is presented firstly. NLOS error correction is implemented subsequently. Finally, GNSS positioning is conducted by WLS method using the healthy and corrected pseudorange measurements.

4.1 NLOS Correction Based on Real-time Point Clouds

In terms of the measurements from GNSS receiver, each pseudorange measurement ρ_n is written as follows [33].

$$\rho_n = R_n + c(\delta t^{\mathrm{r}} - \delta t_n^{\mathrm{sv}}) + I_n + T_n + \varepsilon_n \tag{8}$$

where $\boldsymbol{R_n}$ is the geometric range between the satellite and the GNSS receiver. $\boldsymbol{\delta t_n^{sv}}$ denotes the satellite clock bias. $\boldsymbol{\delta t^{r}}$ indicates the receiver clock bias. $\boldsymbol{I_n}$ represents the ionospheric delay distance; $\boldsymbol{T_n}$ indicates the tropospheric delay distance. $\boldsymbol{\varepsilon_n}$ represents the errors caused by the multipath effects, NLOS receptions, receiver noise, antenna delay, and so on. In this paper, we focus on mitigating the NLOS errors caused by environment buildings. The NLOS error model is proposed in [6]. $\boldsymbol{\alpha}$ represents the distance from receiver to the building. $\boldsymbol{\theta_{ele}}$ represents the elevation angle of GNSS signal. Assuming the building is vertical to the ground and GNSS signal reflection satisfied the law of reflection. The direction of real signal transmission is parallel to the direction of expected signal transmission. The route distance difference $\boldsymbol{\gamma}$ between the reflected signal and expected signal is indicated as follows [6]:

$$\gamma = \gamma_1 + \gamma_2 \tag{9}$$

$$\gamma_1 = \alpha sec\theta_{ele} \tag{10}$$

$$\gamma_2 = \gamma_1 \cos(\theta_1 + \theta_2) \tag{11}$$

Thus, the NLOS error can be calculated with azimuth and elevation angle, and the distance from receiver to the building causing the reflection. In this paper, the distance from the GNSS receiver is directly provided by the 3D LiDAR point clouds. The detailed NLOS correction implementation can be found in the previous work of our team in [30].

4.2 GNSS Positioning Based on corrected Pseudorange Measurements

The clock bias between GNSS receiver and satellites is usually represented by the pseudorange measurements. The equation linking the receiver position and satellite can be structured as the following formula using least square (LS) method:

$$\hat{\boldsymbol{x}} = (\boldsymbol{G^T G})^{-1} \boldsymbol{G^T \rho} \tag{12}$$

where $\boldsymbol{G}$ represents the observation matrix and is structured by unit LOS vectors between GNSS receivers' position and satellites position. $\hat{\boldsymbol{x}}$ indicates the estimated receiver position and $\boldsymbol{\rho}$ denotes the pseudorange measurements vector. Conventionally, to better represent the reliability of each measurement based on the information measured by receiver, weightings of each measurement are needed. Function to calculate the weighting by integrating the measurement C/N_0 and satellite elevation angle is expressed as $\boldsymbol{W}$ [34]. Finally, GNSS receiver position can be estimated using WLS method as:

$$\hat{\boldsymbol{x}} = (\boldsymbol{G^T W G})^{-1} \boldsymbol{G^T W \rho} \tag{13}$$

5. EXPERIMENT EVALUATION

5.1 Experiment Setup

The sensor setup is shown in Figure 8. The u-blox M8T receiver is used to collect raw GPS/BeiDou measurements. 3D LiDAR sensor, Velodyne 32, is employed to provide the real-time point clouds scanned from the surroundings. Both u-blox receiver and 3D LiDAR are installed on top of a vehicle during the experiment. The sky-pointing camera is installed near the 3D LiDAR (shown in right panel of Figure 8). A dynamic experiment is conducted in urbanized area in Hong Kong with buildings on both sides, which can be seen in Figure 9. The blue curve denotes the tested trajectory. The ground truth is generated by NovAtel SPAN-CPT (RTK GNSS/INS integrated navigation system with fiber optics gyroscopes). To verify the effectiveness of the proposed method, four positioning solutions are compared:

- Least square (LS) positioning
- Weighted least square (WLS) positioning.
- WLS positioning + NLOS exclusion (WLS-NE): exclude all the detected NLOS measurements.

- WLS positioning + NLOS correction (WLS-NC): detect and correct NLOS measurements.

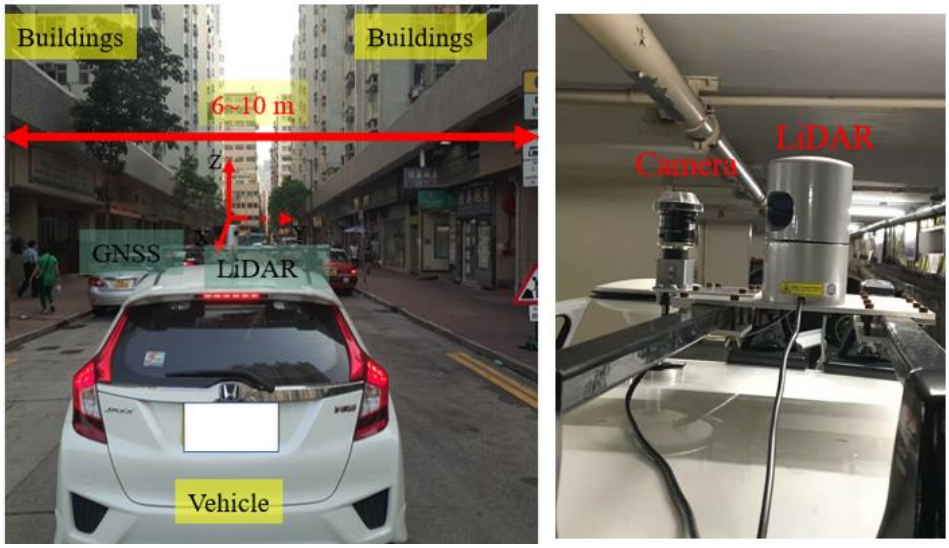

Fig.8 The sensors setup of the vehicle: GNSS and LiDAR sensors are installed on the top of the vehicle.

Fig.9 Environment that the data was collected in an urbanized road with buildings at both sides of the street.

5.2 Comparison of Different GNSS Positioning Solutions

The experiment results of GNSS positioning using the four methods are shown in TABLE 1. 69.26 meters of mean positioning error is obtained during the test using least square method with a significantly large standard deviation, 34.57 meters. Moreover, only about 5.38% of the positioning errors are less than 15 meters. Approximately 68.45% of the results possess errors more than 40 meters. With the aid of weighting for each measurement, the mean positioning error decreases dramatically to 22.01. Moreover, the overall positioning errors fluctuate in a smaller range, 7.61 meters. The percentage of positioning errors less than 15 and 30 meters increase to 41.98% and 95.41%, respectively. These improved results show that the weighting for each satellite plays a significant role in improving GNSS positioning. As the NLOS satellites are detected using the proposed method, the conventional solution is to exclude the NLOS satellites. The mean GNSS positioning error increases from 22.01 to 24.99 meters after the NLOS exclusion. Moreover, the standard deviation increases slightly. 10.76% of the results have a positioning error more than 40 meters. This result shows that the NLOS exclusion is not preferable in this urban scenario. The main reason for the worsen results is due to the distorted satellite distribution. In some extreme cases, NLOS exclusion can cause lack of satellites for GNSS positioning calculation, as at least 5 satellites are needed for GPS/BeiDou positioning. After applying the proposed NLOS correction method, the positioning error decreases from 22.01 (WLS) to 14.96 meters. Moreover, the standard deviation slightly decreases from 7.61 to 6.06. About 77.69% of the results have a positioning error less than 15 meters. 100% of the errors are smaller than 30 meters. This shows that the proposed method can obtain improved performance. The main

reason of the improvement is due to the NLOS correction. In fact, the NLOS measurements involve the additional transmission delay due to the signal reflection. The proposed method corrects the additional delay.

The Skyplot is shown in Figure 10, which is generated based on detected satellites visibilities. In total, there are 9 satellites (GPS/BeiDou) and 4 NLOS satellites (satellite 12,25, 31, 99) are received. The NLOS satellites are detected using the proposed method in this paper. As we can see from TABLE 1, the remaining positioning error is still about 15 meters. The remaining error can be caused by the multipath effects from satellites with high elevation angles (for example, the satellite 24, 92, 20, 21, 96).

The detailed positioning results are shown in Figure 11. The top panel indicates the satellites numbers available for GNSS positioning during the test. In some epochs, the number of satellites available is quite small (8 satellites at epoch 60). The bottom panel indicates the positioning results using WLS and WLS-NC methods. We can find that the positioning is improved from almost throughout the test. Interestingly, we can find that there is an offset between the blue curve (proposed) and the red curve (WLS) which is actually caused by the proposed method. This again verifies that proposed method can effectively detect the NLOS and even correct the NLOS measurements.

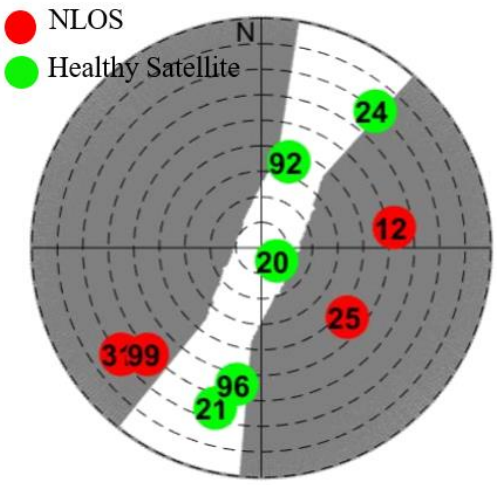

Fig.10 Illustration of Skyplot which indicates the satellites distribution during the dynamic experiment. Green circle represents the satellites that are healthy. Red circle denotes the NLOS satellites.

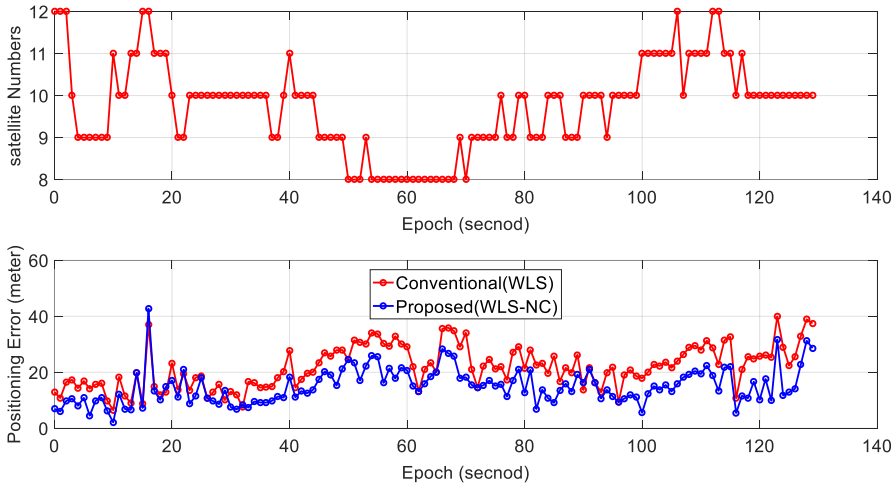

Fig.11 Experimental results of WLS and WLS-NC, which depicted in red and blue dots, respectively. The top panel inciates the numbers of satellites used. Bottom panel indicates the 3D positioning errors.

TABLE.1 POSITIONING PERFORMANCE OF THE FOUR METHODS (IN THE UNIT OF METER)

All data	LS	WLS	WLS-NE	WLS-NC

Mean error	69.26	22.01	24.99	14.96
Std	34.57	7.61	14.69	6.06
Percentage (<15 meters)	5.38%	41.98%	44.62%	77.69%
Percentage (<30 meters)	29.23%	95.41%	82.31%	100%
Percentage (>40 meters)	68.45%	0%	10.76%	0%

TABLE.2 VALUE OF CORRECTED PSEUDORANGE (IN THE UNIT OF METER)

NLOS Satellite PRN	Elevation Angle	C/N_0	Pseudorange Correction
12	37.24°	27 dB-Hz	5.08 m
25	46.67°	19 dB-Hz	5.71 m
31	20.94°	22 dB-Hz	10.32 m
99	28.78°	24 dB-Hz	12.45 m

Based on the proposed NLOS detection and correction method, the pseudorange correction values are shown in TABLE 2. The information is captured from one epoch of the test with 4 NLOS receptions (satellites 12, 25, 31 and 99). The pseudorange corrections for satellites 12 and 25 are 5.08 and 5.71 meters, respectively. The pseudorange corrections for satellites (satellite 31, 99) in lower elevation angles introduce larger corrections. 12.45 meters of correction are calculated for satellite 99. This result denotes that the NLOS satellites with lower elevation angle can introduce larger error in pseudorange measurements. In other word, more additional transmission delay is obtained.

6. CONCLUSIONS AND FUTURE WORK

Insufficient positioning accuracy and robustness is one of the main problems preventing the arrival of autonomous vehicles. As mentioned in [8], NLOS is the major component causing unsatisfactory GNSS positioning result in super-urbanized cities. NLOS exclusion is a commonly studied idea to improve GNSS positioning and some improvements can be obtained in sub-urban scenarios. From the result presented in TABLE 1, NLOS exclusion can result in larger positioning errors (24.99 meters) in urbanized area. NLOS correction is needed to radically alleviate the presence of NLOS receptions.

To mitigate the NLOS errors without relying on the time-consuming ray-tracing process, this paper proposes to detect the NLOS receptions and correct the NLOS measurements with the aid of real-time point clouds. The monocular camera is firstly applied to capture the sky view image. Then the sky view is segmented, and satellites are projected into the segmented image. The NLOS satellites are detected using a proposed searching method. Instead of excluding the NLOS receptions from GNSS positioning calculation, the NLOS measurements are corrected using a NLOS model. Both the healthy and corrected pseudorange measurements are employed to conduct the GNSS positioning. The accuracy is improved from 22.01 (WLS) to 14.96 meters which shows the effectiveness of the proposed method.

In the near future, fish-eye camera with broader field of view (FOV) will be applied to capture the surroundings. Moreover, the remaining mean GNSS positioning error is still about 15 meters. The error caused by the multipath effects will be analyzed in the future.

REFERENCES

[1] C. Urmson *et al.*, "Autonomous driving in urban environments: Boss and the Urban Challenge," (in English), *Journal of Field Robotics*, vol. 25, no. 8, pp. 425-466, Aug 2008.

[2] J. Levinson and S. Thrun, "Robust Vehicle Localization in Urban Environments Using Probabilistic Maps," (in English), *2010 Ieee International Conference on Robotics and Automation (Icra)*, pp. 4372-4378, 2010.

[3] Y. Gu, L.-T. Hsu, and S. Kamijo, "GNSS/onboard inertial sensor integration with the aid of 3-D building map for lane-level vehicle self-localization in urban canyon," *IEEE Transactions on Vehicular Technology*, vol. 65, no. 6, pp. 4274-4287, 2016.

[4] A. Fernandez *et al.*, "GNSS/INS/LiDAR integration in urban environment: Algorithm description and results from ATENEA test campaign," in *Satellite Navigation Technologies and European Workshop on GNSS Signals and Signal Processing,(NAVITEC), 2012 6th ESA Workshop on*, 2012, pp. 1-8: IEEE.

[5] W. Wen, G. Zhang, and L.-T. Hsu, "Exclusion of GNSS NLOS receptions caused by dynamic objects in heavy traffic urban scenarios using real-time 3D point cloud: An approach without 3D maps," in *Position, Location and Navigation Symposium (PLANS), 2018 IEEE/ION*, 2018, pp. 158-165: IEEE.

[6] L.-T. Hsu, "Analysis and modeling GPS NLOS effect in highly urbanized area," *GPS solutions*, vol. 22, no. 1, p. 7, 2018.

[7] S. H. Kong, "Statistical Analysis of Urban GPS Multipaths and Pseudo-Range Measurement Errors," *IEEE Transactions on Aerospace & Electronic Systems*, vol. 47, no. 2, pp. 1101-1113, 2011.

[8] J. Breßler, P. Reisdorf, M. Obst, and G. Wanielik, "GNSS positioning in non-line-of-sight context—A survey," in *Intelligent Transportation Systems (ITSC), 2016 IEEE 19th International Conference on*, 2016, pp. 1147-1154: IEEE.

[9] P. François, B. David, and M. Florian, "Non-Line-Of-Sight GNSS signal detection using an on-board 3D model of buildings," in *ITS Telecommunications (ITST), 2011 11th International Conference on*, 2011, pp. 280-286: IEEE.

[10] P. D. Groves, Z. Jiang, L. Wang, and M. K. Ziebart, "Intelligent urban positioning using multi-constellation GNSS with 3D mapping and NLOS signal detection," 2012.

[11] S. Peyraud *et al.*, "About Non-Line-Of-Sight Satellite Detection and Exclusion in a 3D Map-Aided Localization Algorithm," *Sensors*, vol. 13, no. 1, pp. 829-847, 2013.

[12] L. Wang, P. D. Groves, and M. K. Ziebart, "Urban positioning on a smartphone: Real-time shadow matching using GNSS and 3D city models," 2013: The Institute of Navigation.

[13] L. Wang, P. D. Groves, and M. K. Ziebart, "GNSS shadow matching: Improving urban positioning accuracy using a 3D city model with optimized visibility scoring scheme," *Navigation*, vol. 60, no. 3, pp. 195-207, 2013.

[14] L. Wang, P. D. Groves, and M. K. Ziebart, "Smartphone shadow matching for better cross-street GNSS positioning in urban environments," *The Journal of Navigation*, vol. 68, no. 3, pp. 411-433, 2015.

[15] P. D. Groves and M. Adjrad, "Likelihood-based GNSS positioning using LOS/NLOS predictions from 3D mapping and pseudoranges," *GPS Solutions*, journal article vol. 21, no. 4, pp. 1805-1816, October 01 2017.

[16] M. Adjrad and P. D. Groves, "Intelligent Urban Positioning: Integration of Shadow Matching with 3D-Mapping-Aided GNSS Ranging," *Journal of Navigation*, vol. 71, no. 1, pp. 1-20, 2018.

[17] L.-T. Hsu, Y. Gu, and S. Kamijo, "3D building model-based pedestrian positioning method using GPS/GLONASS/QZSS and its reliability calculation," (in English), *GPS Solutions*, vol. 20, no. 3, pp. 413–428, 2016.

[18] S. Miura, L.-T. Hsu, F. Chen, and S. Kamijo, "GPS error correction with pseudorange evaluation using three-dimensional maps," *IEEE Transactions on Intelligent Transportation Systems*, vol. 16, no. 6, pp. 3104-3115, 2015.

[19] M. Obst, S. Bauer, P. Reisdorf, and G. Wanielik, "Multipath detection with 3D digital maps for robust multi-constellation GNSS/INS vehicle localization in urban areas," in *Intelligent Vehicles Symposium (IV), 2012 IEEE*, 2012, pp. 184-190: IEEE.

[20] T. Suzuki and N. Kubo, "Correcting GNSS multipath errors using a 3D surface model and particle filter," *Proc. ION GNSS+ 2013*, 2013.

[21] Y.-W. Lee, Y.-C. Suh, and R. Shibasaki, "A simulation system for GNSS multipath mitigation using spatial statistical methods," *Computers & Geosciences*, vol. 34, no. 11, pp. 1597-1609, 2008.

[22] D. Maier and A. Kleiner, "Improved GPS sensor model for mobile robots in urban terrain," in *Robotics and Automation (ICRA), 2010 IEEE International Conference on*, 2010, pp. 4385-4390: IEEE.

[23] A. Shetty and G. X. Gao, "Covariance Estimation for GPS-LiDAR Sensor Fusion for UAVs," in *ON GNSS+ 2017, Portland, OR, USA*, 2017.

[24] J. I. Meguro, T. Murata, J. I. Takiguchi, Y. Amano, and T. Hashizume, "GPS multipath mitigation for urban area using omnidirectional infrared camera," *IEEE Transactions on Intelligent Transportation Systems*, vol. 10, no. 1, pp. 22-30, 2009.

[25] T. Suzuki, M. Kitamura, Y. Amano, and T. Hashizume, "High-accuracy GPS and GLONASS positioning by multipath mitigation using omnidirectional infrared camera," in *IEEE International Conference on Robotics and Automation*, 2011, pp. 311-316.

[26] J. S. Sánchez, A. Gerhmann, P. Thevenon, P. Brocard, A. B. Afia, and O. Julien, "Use of a FishEye camera for GNSS NLOS exclusion and characterization in urban environments," in *ION ITM 2016, International Technical Meeting*, 2016: ION.

[27] P. V. Gakne, "Improving the Accuracy of GNSS Receivers in Urban Canyons using an Upward-Facing Camera," PhD Thesis, Geomatics Engineering, University of Calgary. doi: dx. doi. org …, 2018.

[28] P. V. Gakne and K. O'Keefe, "Tightly-Coupled GNSS/Vision Using a Sky-Pointing Camera for Vehicle Navigation in Urban Areas," *Sensors*, vol. 18, no. 4, p. 1244, 2018.

[29] R. Mur-Artal, J. M. M. Montiel, and J. D. Tardos, "ORB-SLAM: a versatile and accurate monocular SLAM system," *IEEE Transactions on Robotics*, vol. 31, no. 5, pp. 1147-1163, 2015.

[30] G. Z. Weisong Wen, Li-ta Hsu, "Correcting GNSS NLOS by 3D LiDAR and Building Height," presented at the ION GNSS+, 2018, Miami, Florida, USA., 2018.

[31] J. Marshall, "Creating and viewing skyplots," *GPS solutions*, vol. 6, no. 1-2, pp. 118-120, 2002.

[32] G. Bradski and A. Kaehler, "OpenCV," *Dr. Dobb's journal of software tools,* vol. 3, 2000.
[33] E. Kaplan and C. Hegarty, *Understanding GPS: principles and applications*. Artech house, 2005.
[34] E. Realini and M. Reguzzoni, "goGPS: open source software for enhancing the accuracy of low-cost receivers by single-frequency relative kinematic positioning," *Measurement Science and technology,* vol. 24, no. 11, p. 115010, 2013.

View publication stats